Analysis of thermospheric characteristic anomalies from 2021 Mw 7.5 Peru earthquake

Xitong Xu
College of Geo-exploration Science and Technology, Jilin University
British Geological Survey
Changchun, China
xuxitong.2007@163.com

Shengbo Chen*
College of Geo-exploration Science and Technology, Jilin University
Changchun, China

Lei Wang
British Geological Survey
Keyworth, United Kingdom

***Abstract*—This study investigates the relationship between seismic activity and thermospheric anomalies related to the 2021 Mw 7.5 Peru earthquake. Utilizing data from the National Center Environmental Prediction (NCEP) reanalysis and the Ionospheric Connection Explorer (ICON) satellite with the Michelson Interferometer for Global High-resolution Thermospheric Imaging (MIGHTI), temperature and vector wind anomalies were analyzed. Seismic thermal anomalies in the lower atmosphere were found to precede significant temperature fluctuations in the thermosphere, displaying a bottom-up propagation pattern. Additionally, vector wind analysis revealed a strengthening radial component originating from the epicenter, indicating energy propagation from the earthquake source. The observed vertical perturbations and horizontal disturbances in the thermosphere provide evidence of the link between seismic activity and thermospheric disturbances, advancing our understanding of the mechanisms underlying Lithosphere Atmosphere-Ionosphere Coupling (LAIC). These findings contribute to LAIC research and provide valuable insights into the processes involved in seismic-related ionospheric disturbances.**

Keywords-thermosphere; seismic anomaly; earthquake; temperature; vector wind

I. INTRODUCTION

The topic of prominent alterations in the lithosphere, atmosphere, and ionosphere, potentially linked to seismic activity, has remained a persistent focus for numerous researchers. A multitude of investigations have presented empirical evidence supporting the interpretation of diverse pre-seismic and post-seismic comprehensive disturbances as manifestations of the Lithosphere Atmosphere-Ionosphere Coupling (LAIC) [1-2]. To date, many researches have been conducted to elucidate the genesis of LAIC, but this subject remains ripe for further exploration. This is related to the lack of evidence for a large number of intermediate transmission process [3]. In the context spanning from the lithosphere to the ionosphere, a substantial vertical spatial extent should be considered, while the range of intense earthquake preparation activities displays considerable breadth, thereby augmenting the extent of horizontal effects. Therefore, a comprehensive investigation of seismic anomalies across various spatial scales becomes indispensable for a thorough understanding [4]. The investigation of thermosphere characteristic changes can reveal the propagation progress of anomalies from the lower atmosphere to the ionosphere. However, there are few researches on thermospheric seismic anomalies, which can not provide support for LAIC. Thermal anomalies are causally associated with fault systems and linear structures within the Earth's crust, serving as the origination of LAIC [3,5]. As the important characteristics for understanding the electrodynamics in the thermosphere, temperature and vector wind can serve as key indicators of the migration of neutral gas [6]. Therefore, we can further understand the effect of earthquakes on circulation by detecting the anomalies of temperature and vector wind. The study investigates the thermospheric characteristic anomalies related to the Mw 7.5 Peru earthquake (4.467° S, 76.813° W) on November 28, 2021. We utilize seismic thermal anomalies as a reference to conduct comparative analysis of thermospheric characteristics, investigating the influence on thermospheric circulation during the seismic preparation phases, thereby providing substantial evidence for the potential mechanism of LAIC.

II. DATA AND METHODS

A. Reanalysis data and satellite data

In this study, we investigate the temperature anomalies in the lower atmosphere and the characteristic anomalies in the thermosphere. The air temperature data are collected from National Center Environmental Prediction (NCEP) reanalysis data with 6-hour temporal resolution at the ground surface and 26 isobaric levels [7]. The ground surface and five isobaric

levels are selected for anomaly detection. Given the altitude of epicenter, five isobaric (i.e., 900hPa, 850hPa, 800hPa, 750hPa, 700hPa) with the shortest distance above the epicenter are extracted.

As the newest addition to NASA's Heliophysics satellite constellation, the Ionospheric Connection Explorer (ICON) with a 27-degree inclination orbit come on a mission to explore the association between Earth's atmosphere and the space environment [8]. MIGHTI (The Michelson Interferometer for Global High-resolution Thermospheric Imaging) is carried on board the ICON satellite and utilizes five distinct wavelength channels [9]. This configuration enables MIGHTI to effectively measure the shape of the band and specify a background radiance that is subsequently subtracted from the signal [10]. By being deployed on the ICON satellite, MIGHTI gains the advantage of a comprehensive global perspective, enabling the investigation and analysis of complex thermospheric dynamics on a broader scale. We apply temperature data and cardinal vector wind data from MIGHTI to identify anomalous behavior in the thermosphere. Note that temperature sampling mainly ranges from 90-110 km, whereas the samples of cardinal vector wind with an altitude less than 110 km are mainly below 95 km in the study area (i.e., from -9° S to 1° N, and from -82° W to -72° W).

B. *Anomaly detection in the lower atmosphere based on tidal force*

Tidal Force Fluctuation Analysis (TFFA) is a method to detect seismic thermal anomalies in the lower atmosphere based on tidal force periods. The feasibility of identifying seismic thermal anomalies using TFFA has been demonstrated by researchers, and the details of TFFA are discussed in previous studies [11-14]. Also, the procedure for calculating tidal force potential was detailed described by Zhang et al. [15]. The spatial parameters used in TFFA include the epicenter location and the active faults, as shown in Figure 1. In order to enhance the clarity of the anomaly chain propagation, we consider a longer time span, including eight tidal cycles (from September 28, 2021 to January 24, 2022).

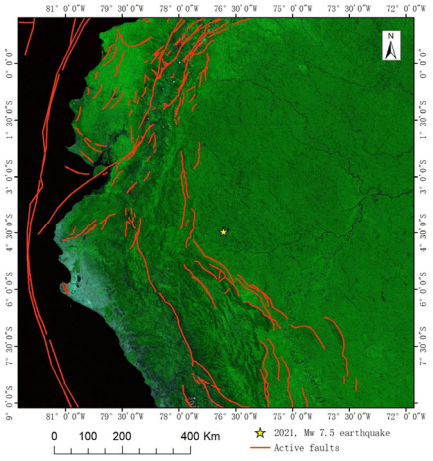

Figure 1. Geographical location of 2021 Peru earthquake. The red lines represent active faults.

C. *Anomaly detection in the lower atmosphere based on tidal force*

Taking into account the vertical distribution of temperature and vector wind data, the temperature sampling is segmented into four sub-ranges based on altitude (i.e., 90-95 km, 95-100 km, 100-105 km, and 105-110 km), whereas the vector wind data is comprehensively analyzed over the 90-110 km range. Two data sets are brought together to a time scale identical to the eight tidal force periods.

The median temperature value (μ_d) is extracted for each day within the study area throughout the research period. The mean of these daily median values is computed as the background value (m) for the entire research period. This background value is then utilized as described in Eq (1):

$$\Delta T_d = (\mu_d - m)/m \tag{1}$$

where, μ_d is the median temperature of the dth day, and ΔT_d is the percentage temperature difference relative to the background value on the d th day. The aforementioned procedure is executed for each of the four altitude sub-ranges.

Due to the vertical distribution of wind data sampling, the data of 90-110 km is calculated as a whole. In the horizontal dimension, the study area is partitioned into grids measuring 1° ×1° . In each cell, the daily mean values of wind velocity, wind direction, radial component of wind velocity and tangent component of wind velocity are calculated. The calculation of the wind velocity components is based on the center point location of each cell. Then, the radial and tangent components of wind velocity are analyzed, as described in Eq (2):

$$\begin{cases} \Delta Vr_d = Vr_d - Vr_{mean} \\ \Delta Vt_d = Vt_d - Vt_{mean} \end{cases} \tag{2}$$

where Vr_d is the average value of radial component of wind velocity for all cells on the dth day, Vr_{mean} is the mean value of Vr_d over the research period, Vt_d is the average value of tangent component of wind velocity for all cells on the dth day, Vt_{mean} is the mean value of Vt_d over the research period.

In addition, the upper and lower boundaries of ΔT_d, ΔVr_d, ΔVt_d are calculated according to the mean (σ) and standard deviation (std) to identify the anomalous trend. Here, we consider the variation of temperature fluctuations at different altitudes, necessitating the application of a moderate constraint parameter (q) to effectively limit the range of boundaries. In the past studies on the relationship between the characteristics of the upper atmosphere and earthquakes, this constraint parameter (q) is commonly set to 1.5 [16, 17], thus we adopt this established value as well.

$$\begin{cases} Boundary_{up} = \sigma + q \times \text{std} \\ Boundary_{low} = \sigma - q \times \text{std} \end{cases} \tag{3}$$

III. RESULT AND DISCUSSION

Seismic thermal anomalies in the lower atmosphere were detected over three intervals, as shown in Figure 2. The initial two thermal anomalies exhibit relatively low intensity, whereas the thermal anomaly significantly intensifies subsequent to the earthquake. This observation indicates a gradual intensification in seismic thermal anomalies during earthquake preparation

Identify applicable sponsor/s here. *(sponsors)*

phases. The temporal and spatial pattern is in concurrence with findings reported in previous studies [13,16].

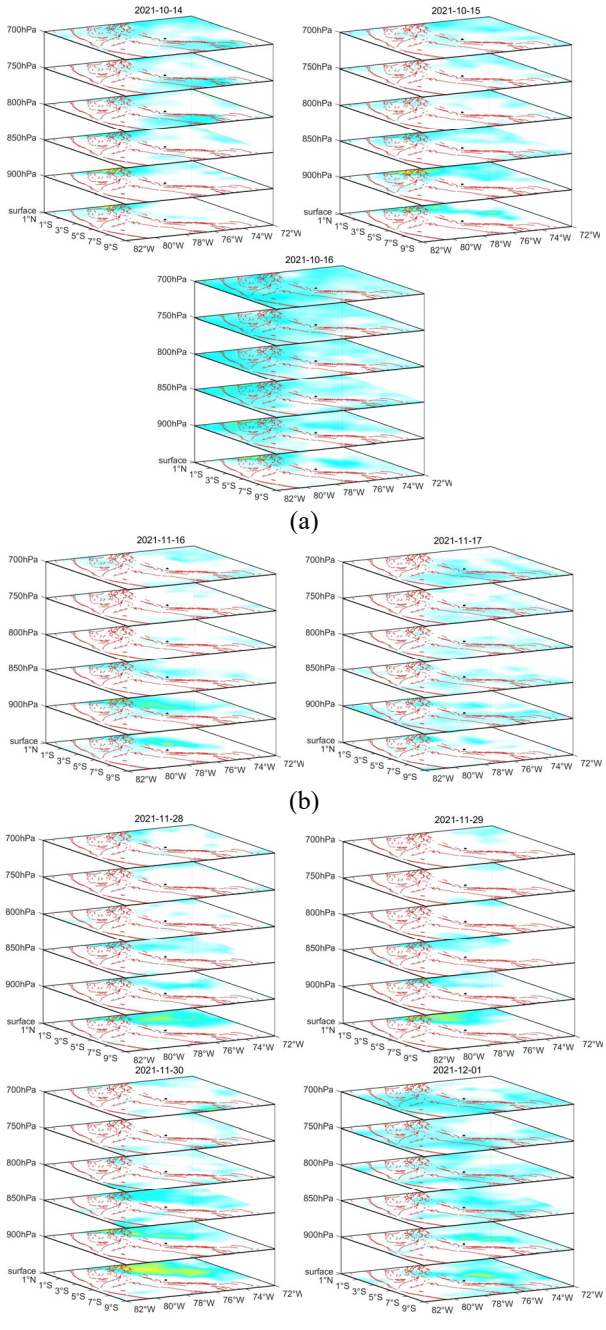

Figure 2. Seismic thermal anomalies during three intervals: (a) October 14-16, 2021, (b) November 16-17, 2021, and (c) November 28-December 1, 2021.

The statistical analysis of thermospheric temperature reveals intriguing patterns (Figure 3). The temperature exhibits relative stability in the altitude range of 90 km to 105 km, whereas a substantial enhancement in fluctuation is observed between 105 km and 110 km. This is related to the increasing intensity of turbulent movements [18]. It is evident that the positive anomalies of temperature display two vertical transfer chains that gradually uplift over time. The time of the two anomaly chains is very close to the time of seismic thermal anomalies. The timing of these two anomaly chains closely aligns with the occurrence of the first and second seismic thermal anomalies, and both chains demonstrate a bottom-up propagation pattern. Note that at the layer of 90-95 km altitude, the temperature rise peak through a gradual process, rather than an abrupt onset. This finding is consistent with the trend of seismic thermal anomalies suggesting that the effects of earthquake preparation on the lower atmosphere act in a similar way on the thermosphere.

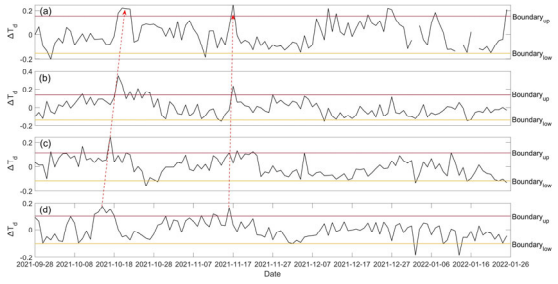

Figure 3. Temperature variation at different altitude ranges: (a) 90-95 km, (b) 95-100 km, (c) 100-105 km and (d) 105-110 km.

The observed temperature variation underscores the temporal and vertical spatial distribution of anomalies, necessitating the execution of vector wind analysis to elucidate the temporal and horizontal spatial distribution. Figure 4 presents the variation trend of radial and tangent components of wind velocity during the research period. We can note two significant increase of the radial component, which corresponds to stronger wind velocity from the epicenter. Concurrently, the tangential component exhibits a declining trend. These two abrupt changes coincide with the time of the first and third seismic thermal anomalies. After the numerical series of radial component and tangent component, further horizontal spatial observations are necessary to verify the relationship between vector wind variation and the earthquake. Then, we select the two days (i.e., October 18, 2021, and November 28, 2021) when the radial component reaches its peak to generate the vector wind map, as shown in Figure 5. It can be seen that the vector wind of the cells with data presents a clear tendency to diverge outward from the epicenter. The results are in agreement with the previous study that reported the outward diffusion of thermospheric vector wind after large earthquakes [18]. This provides obvious evidence for the seismic-related change of dynamic characteristic of the thermosphere.

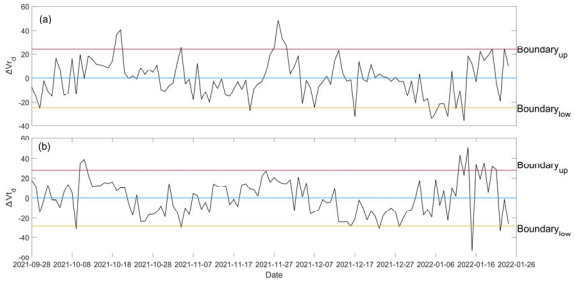

Figure 4. The variation of (a) radial component and (b) tangent component of wind velocity within 90-110 km.

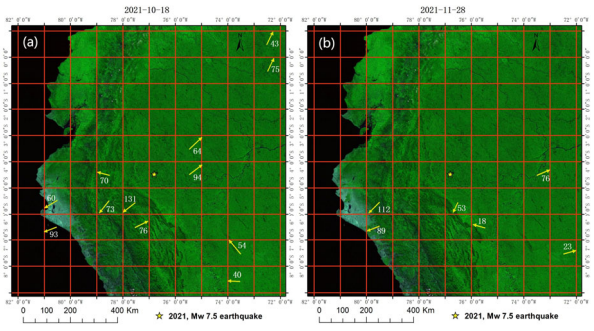

Figure 5. Wind velocity map near the epicenter on (a) October 18, 2021, and (b) November 28, 2021.

The temperature and vector wind in the thermosphere exhibit noticeable disturbances when seismic thermal anomalies occur in the lower atmosphere. This signifies a distinct and continuous process in the upward propagation of seismic anomalies for the lower atmosphere. Previous study has reported that seismic thermal anomalies induce vertical air mass ascent and give rise to air pressure gradients in the lower atmosphere [14]. It appears that this influence propagates up to thermosphere and even higher altitudes. Observations of temperature and vector wind in the thermosphere indicates that seismic thermal anomalies cause turbulence enhancement at the heights of mesopause. This effect may further lead to changes in various ionospheric characteristics [19,20]. In this way, the formation mechanism of seismic-related ionospheric disturbances observed by satellite in recent years can be investigated. This study opens avenues for exploring the underlying process of LAIC.

IV. Conclusions

The temperature and vector wind in the thermosphere exhibit noticeable disturbances when seismic thermal anomalies occur in the lower atmosphere. This signifies a distinct and continuous process in the upward propagation of seismic anomalies for the lower atmosphere. Previous study has reported that seismic thermal anomalies induce vertical air mass ascent and give rise to air pressure gradients in the lower atmosphere [13]. It now appears that this influence can propagate up to thermosphere and even high altitudes. Observations of temperature and vector wind in the thermosphere indicates that seismic thermal anomalies cause turbulence enhancement at the heights of mesopause. This effect may further lead to changes in various ionospheric characteristics [17,18]. In this way, the formation mechanism of seismic-related ionospheric disturbances observed by satellite in recent years can be investigated. This study opens avenues for exploring the underlying process of LAIC.

References

[1] M. Shah, A. C. Aibar, M. A. Tariq, J. Ahmed, and A. Ahmed, "Possible ionosphere and atmosphere precursory analysis related to Mw> 6.0 earthquakes in Japan," Remote Sensing of Environment, vol. 239, p. 111620, 2020.

[2] D. Marchetti *et al.*, "Pre-earthquake chain processes detected from ground to satellite altitude in preparation of the 2016–2017 seismic sequence in Central Italy," *Remote Sensing of Environment,* vol. 229, pp. 93-99, 2019.

[3] S. Pulinets and D. Ouzounov, "Lithosphere–Atmosphere–Ionosphere Coupling (LAIC) model–An unified concept for earthquake precursors validation," *Journal of Asian Earth Sciences,* vol. 41, no. 4-5, pp. 371-382, 2011.

[4] D. Marchetti *et al.*, "Possible Lithosphere-Atmosphere-Ionosphere Coupling effects prior to the 2018 Mw= 7.5 Indonesia earthquake from seismic, atmospheric and ionospheric data," *Journal of Asian Earth Sciences,* vol. 188, p. 104097, 2020.

[5] A. A. Tronin, M. Hayakawa, and O. A. Molchanov, "Thermal IR satellite data application for earthquake research in Japan and China," *Journal of Geodynamics,* vol. 33, no. 4-5, pp. 519-534, 2002.

[6] J. Lei, J. P. Thayer, A. G. Burns, G. Lu, and Y. Deng, "Wind and temperature effects on thermosphere mass density response to the November 2004 geomagnetic storm," *Journal of Geophysical Research: Space Physics,* vol. 115, no. A5, 2010.

[7] R. Kistler *et al.*, "The NCEP/NCAR 50-year reanalysis: Documentation and monthly-means CD-ROM," *Bull. Am. Meteorol. Soc,* vol. 82, pp. 1520-0477, 2001.

[8] T. J. Immel *et al.*, "The ionospheric connection explorer mission: Mission goals and design," *Space Science Reviews,* vol. 214, pp. 1-36, 2018.

[9] C. R. Englert *et al.*, "Michelson interferometer for global high-resolution thermospheric imaging (MIGHTI): instrument design and calibration," *Space science reviews,* vol. 212, pp. 553-584, 2017.

[10] J. M. Harlander *et al.*, "Michelson interferometer for global high-resolution thermospheric imaging (MIGHTI): monolithic interferometer design and test," *Space science reviews,* vol. 212, pp. 601-613, 2017.

[11] W. Ma *et al.*, "Influences of multiple layers of air temperature differences on tidal forces and tectonic stress before, during and after the Jiujiang earthquake," *Remote Sensing of Environment,* vol. 210, pp. 159-165, 2018.

[12] Y. Zhang, Q. Meng, Z. Wang, X. Lu, and D. Hu, "Temperature variations in multiple air layers before the Mw 6.2 2014 Ludian earthquake, Yunnan, China," *Remote Sensing,* vol. 13, no. 5, p. 884, 2021.

[13] X. Xu, S. Chen, Y. Yu, and S. Zhang, "Atmospheric anomaly analysis related to Ms> 6.0 earthquakes in China during 2020–2021," *Remote Sensing,* vol. 13, no. 20, p. 4052, 2021.

[14] X. Xu, S. Chen, S. Zhang, and R. Dai, "Analysis of Potential Precursory Pattern at Earth Surface and the Above Atmosphere and Ionosphere Preceding Two Mw≥ 7 Earthquakes in Mexico in 2020–2021," *Earth and Space Science,* vol. 9, no. 10, p. e2022EA002267, 2022.

[15] X. Zhang, C. Kang, W. Ma, J. Ren, and Y. Wang, "Study on thermal anomalies of earthquake process by using tidal-force and outgoing-longwave-radiation," *Thermal Science,* vol. 22, no. 2, pp. 767-776, 2018.

[16] M. Akhoondzadeh, A. De Santis, D. Marchetti, A. Piscini, and G. Cianchini, "Multi precursors analysis associated with the powerful Ecuador (MW= 7.8) earthquake of 16 April 2016 using Swarm satellites data in conjunction with other multi-platform satellite and ground data," *Advances in Space Research,* vol. 61, no. 1, pp. 248-263, 2018.

[17] A. De Santis *et al.*, "A comprehensive multiparametric and multilayer approach to study the preparation phase of large earthquakes from ground to space: The case study of the June 15 2019, M7. 2 Kermadec Islands (New Zealand) earthquake," *Remote Sensing of Environment,* vol. 283, p. 113325, 2022.

[18] B. Gordiets, Y. N. Kulikov, M. Markov, and M. Y. Marov, "Numeric modeling of warming and cooling a gas in the near Earth space," in *Infrared Spectroscopy of Cosmic Matter and Environment Properties in Space*, vol. 130: Nauka Moscow, 1982, pp. 3-28.

[19] L. Kozak, M. Dzubenko, and V. Ivchenko, "Temperature and thermosphere dynamics behavior analysis over earthquake epicentres from satellite measurements," *Physics and Chemistry of the Earth, Parts A/B/C,* vol. 29, no. 4-9, pp. 507-515, 2004.

[20] E. I. Astafyeva and E. L. Afraimovich, "Long-distance traveling ionospheric disturbances caused by the great Sumatra-Andaman earthquake on 26 December 2004," *Earth, planets and space,* vol. 58, pp. 1025-1031, 2006.